Alma Mater Studiorum Università di Bologna
Archivio istituzionale della ricerca

Application of a Neural-Network-Based Algorithm for the Real-Time Correction of the In-Cylinder Pressure Signal Sensed with a Piezoelectric Washer

27 June 2024

Application of a neural network-based algorithm for the real-time correction of the in-cylinder pressure signal sensed with a piezoelectric washer

Abstract

The objective of this work is to analyze the signal of a piezoelectric washer installed under the spark plug and to compare the combustion metrics determined from such signal to the indexes from a standard piezoelectric sensor for the in-cylinder pressure measurement, considered as the reference in this work.
In the first part of the paper, the spectrum analysis of the piezoelectric washer pressure trace is proposed. It is demonstrated how such signal can be used to measure the main combustion and knock indexes. Nevertheless, due to intrinsic characteristics of the system, the knock index evaluated from the raw pressure trace cannot be directly used to estimate the instantaneous knock intensity. For this reason, a model-based algorithm for the real-time application is developed to calculate a corrective factor of the high-frequency content of the signal. With such algorithm, the logarithmic mean value of the Maximum Amplitude of Pressure Oscillation can be accurately evaluated through an Artificial Neural Network-based algorithm to properly scale the indexes calculated from the washer signal. Such algorithm is further developed with respect to a precedent work of the authors by introducing a new function to account for the intake air temperature and the fuel quality effects on knock indexes, and it needs both some variables provided by the Engine Control Unit and raw washer combustion indexes as inputs.
In the last part of the work, the algorithm is validated at the engine test bench under steady-state and transient conditions by reproducing speed and load profiles.

Keywords: piezoelectric sensors, low-cost piezoelectric sensors, piezoelectric washers, knock, knock index, knock modeling, combustion, combustion modeling, combustion control, neural network, artificial intelligence

Introduction

During the last decades, engine manufactures and researchers invested significant efforts to increase combustion process efficiency and decrease pollutant emissions. One of the widely adopted solutions to reach higher values of mechanical and thermal efficiencies is the so-called downsizing, applied especially in Spark Ignition (SI) engines and coupled with turbocharging and supercharging. This solution leads to reach high pressure and temperature within the combustion chamber and these thermodynamics conditions facilitate abnormal combustions occurrence that generates severe pressure oscillations that can cause serious damage to the combustion chamber components. As well-known from literature [1], the Spark Advance (SA) angle that guarantees Maximum Brake Torque (MBT) should be applied to maximize combustion efficiency, but knock remains one of the main limitations to efficiency increase. Enabling robust and cheap in-cylinder pressure sensing is thus a key step to significantly improve on-board combustion efficiency management. Excluding standard piezoelectric pressure sensors, which cannot be adopted for real on-vehicle applications for cost and reliability reasons [2], the main technologies applied on production engines are the following ones:

- Ionization current (ION)
- Accelerometers
- Microphones

The first system is sensitive to the concentration of molecules that get ionized by heat, making the in-cylinder charge conductive. By applying a voltage difference to the spark plug electrodes, ions concentration can be measured, thus obtaining a signal that can describe the in-cylinder pressure trace [3]. In literature, several authors demonstrated that ION-based controllers can manage combustion phase with good accuracy [4, 5]. It was proven that ION is reliable even for pre-ignition diagnostic [6, 7], misfire detection [8, 9], and Exhaust Gas Recirculation (EGR) estimation [10], because of the capability to catch the Cycle-to-Cycle Variation (CCV).

While ION is a technology suitable for SI engines, the accelerometer mounted on the engine head or block can be used also for Compression Ignition engines. As demonstrated in [11-14], the accelerometric signal can be properly treated to determine some synthetic indexes that are well correlated to the angle of 50% of Mass of Fuel Burnt (MFB50) and the Start of Combustion (SOC). The accelerometer is considered as a robust sensor also for knock intensity measurement, but integral indexes [15] or a model-based approach [16] are needed to reduce the intrinsic noise that characterizes the signal.

Microphone signal is characterized by features that are close to those described for the accelerometer and for this reason its signal can be treated in a similar way [17, 18].

This work presents the development of a model-based, control-oriented algorithm to adjust knock index calculated from the in-cylinder pressure signal estimated with a piezoelectric washer placed between the cylinder head and the production spark plug. It is composed of two thin cases which contain the sensitive part made of the piezoelectric material, as explained in [19]. The final aim is to obtain robust indexes for knock intensity and combustion phase, achieving a good correlation with reference values of Maximum Amplitude of Pressure Oscillation (MAPO) and MFB50, respectively. It is important to mention that the signal coming from the standard piezoelectric sensors and the related combustion and knock indexes are taken as the reference in this work. A robust and accurate estimation of the combustion phase and the knock intensity is the most important step to develop more reliable combustion controllers. Authors demonstrated in [20, 21, 22] that once such indexes are known, the maximum in-cylinder pressure (PMAX) and the Indicated Mean Effective Pressure (IMEP) can be accurately modelled on the entire engine operating range (also for non-traditional combustion concepts such as using water injection) while keeping a high level of accuracy under transient operating conditions, due to the strong dependency on engine load and combustion phase. The identification of a cheap sensor compatible with production requirements can be strategic to deploy innovative combustion controllers, such as the piston damage-based algorithm proposed by the authors in [23, 24], that needs instantaneous combustion phase and knock intensity as inputs.

In the first part of the work the piezoelectric washer signal is studied in the high frequency domain, by analyzing its spectrum. It is shown how the signal of such sensor bears knock-relevant information in the same frequency range considered for the evaluation of MAPO (for frequencies higher than 4 kHz). Nevertheless, due to the intrinsic features of the innovative sensor and its position on the engine head, the so-called Maximum Amplitude of Washer Oscillation (MAWO) knock index, calculated with the same function of MAPO, is not numerically comparable with the corresponding values of the latter. This is the reason why, after studying the statistical properties of MAWO, a model-based algorithm compatible with the Real-Time (RT) execution is developed to adjust the instantaneous MAWO and to make it directly comparable with MAPO. Such algorithm

implements an Artificial Neural Network (ANN) to model the mean value μ of MAPO log-normal distribution [20], and a Feedforward Neural Network (FNN) algorithm is deployed. This kind of model was selected to capture the effects of all the variables that physically affect the abnormal combustion phenomena and their intensity. Moreover, FNNs are suitable for RT applications because these models are based on the solution of simple algebraic functions [25]. In literature, some examples of the implementation of complex ANNs into RT codes can be found [26]. The knock model proposed in [27] is further developed in this work by introducing a new approach for the description of the intake air temperature effects and it is extended even to include the influence of the fuel quality (evaluated as the Research Octane Number, RON). The model-based approach is applied even for PMAX estimation, since the combustion phase is evaluated with high robustness and accuracy, as described by the authors in [21].

In the last section of the paper, the algorithm to scale MAWO values is implemented in a Rapid Control Prototyping (RCP) system and validated at the engine test bench under steady-state and transient conditions. The accuracy of the method is evaluated by correlating indexes obtained from the washer signal with those evaluated from the reference in-cylinder pressure trace.

Experimental Campaign

The experimental campaign is carried out on a V8, 3.9-liter, gasoline direct injection, turbo-charged engine, with exhaust side-mounted spark plugs. The main features of such engine are reported in Table 1.

Table 1. Main engine characteristics.

Displacement	3.9 L (V8 cylinders) - Turbo
Stroke	82 mm
Bore	86.5 mm
Connecting Rod	143 mm
Compression Ratio	9.4
Number of valves per cylinder	4

Experimental tests are performed in two main phases. In the first one, some spark sweeps are carried out and the engine is equipped with a standard piezoelectric sensor for each cylinder. The main features of such sensors are reported in Table 2.

Table 2. Main characteristics of the piezoelectric in-cylinder pressure sensor used.

Sensitivity	37 Pc/bar
Pressure range	0 – 250 bar
Overload	300 bar
Natural frequency	> 215 kHz

Data are collected over the entire engine operating range in different conditions of lambda, intake air temperature and with different types of gasoline (i.e., RON). Figure 1 shows the operating conditions (in the engine speed and load domain) where the engine is operated with RON 95 gasoline and the target lambda equal to 0.75, 1, and the standard mapped values, respectively. Intake air temperature was kept constant and equal to the nominal conditions as defined by the engine manufacturer. Y-axis values are normalized with respect to their maximum, and the same approach is applied to all other combustion indexes for confidentiality reasons. The engine load indicates the trapped air mass per cycle, and thus it represents an index related to the volumetric efficiency.
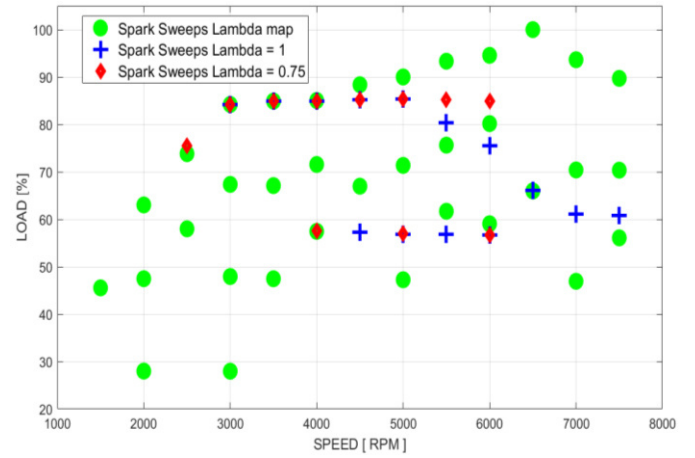

Figure 1. Engine operating conditions tested with different lambda values at the nominal intake air temperature.

Since knock intensity is affected by both the fuel quality and the intake air temperature [27, 28], some tests are carried out with a RON 100 gasoline and at a manifold air temperature higher than nominal (50°C is chosen). Such operating points are shown in Figure 2.
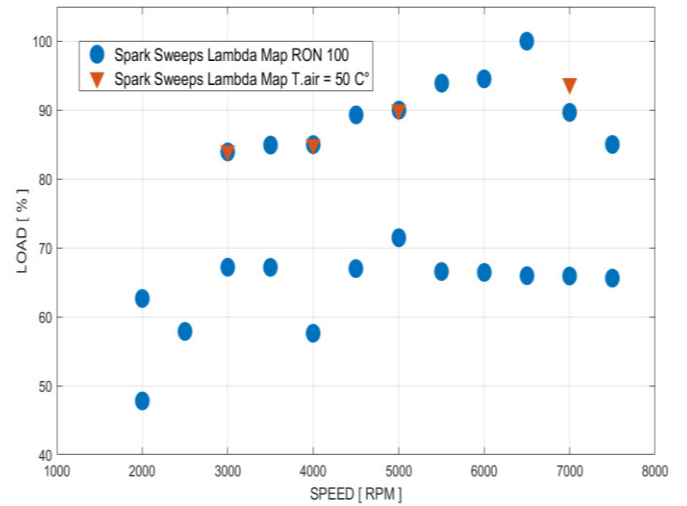

Figure 2. Engine operating conditions tested with RON 100 gasoline and intake air temperature of 50°C (higher than nominal).

For each engine point shown in Figure 1 and Figure 2, and for each spark timing, the in-cylinder pressure signal is recorded for 200 consecutive cycles under steady-state conditions, with a sampling frequency of 200 kHz. Alma Automotive mASTRO charge amplifier and OBI indicating system are used. Combustion indexes are estimated from the low pass filtered pressure curves, with a cut-off frequency of 3 kHz. On the other hand, MAPO index is used to evaluate knock intensity and it is calculated with the following equation:

$$MAPO = \max\left(\left|p_{filt}\right|\right) \tag{1}$$

Where p_{filt} is the band-pass filtered in-cylinder pressure signal. Cut-off frequencies are defined together with the engine manufacturer, and they are not disclosed for confidentiality reasons.

In the second phase of the experimental champaign, three cylinders of the engine are equipped with both the piezoelectric washers and the reference sensors. In this way, the combustion indexes calculated from the washer signal are compared to those obtained from the reference sensor. Also in this case, some spark sweeps are carried out over a wide portion of the engine operating range. These tests are

carried out at mapped lambda, with RON 95 gasoline and nominal intake air temperature. Figure 3 shows such engine operating conditions on the normalized engine speed and load domain.
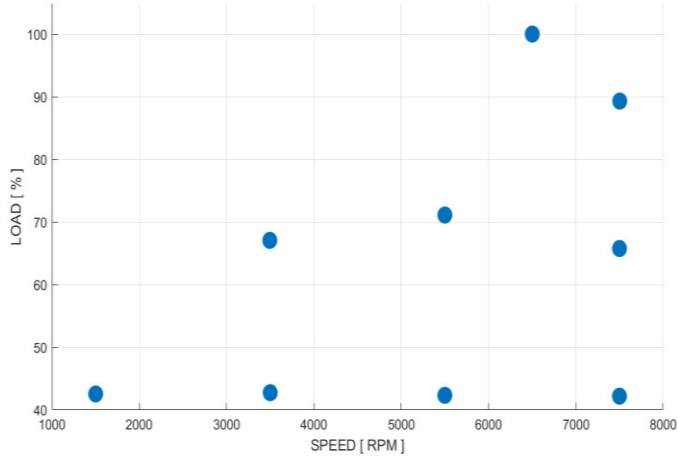

Figure 3. Engine operating conditions tested with the piezoelectric washers installed under the production spark plugs.

Since the washers' sensitivities are unknown a priori, the calibration is carried out starting from the pC/bar ratio of the reference piezoelectric sensor mounted on the same cylinder. As shown in the left-hand graph of Figure 4, where the pressure curves recorded under motored conditions are shown, the gain needs to be recalibrated, as reported in [19, 29]. The gain calibration is performed by multiplying the first sensitivity value with the ratio between the PMAX estimated with the two different sensors. Such ratio is defined by averaging the values calculated under motored and fired conditions. The same approach is applied to all the washers used for this work.
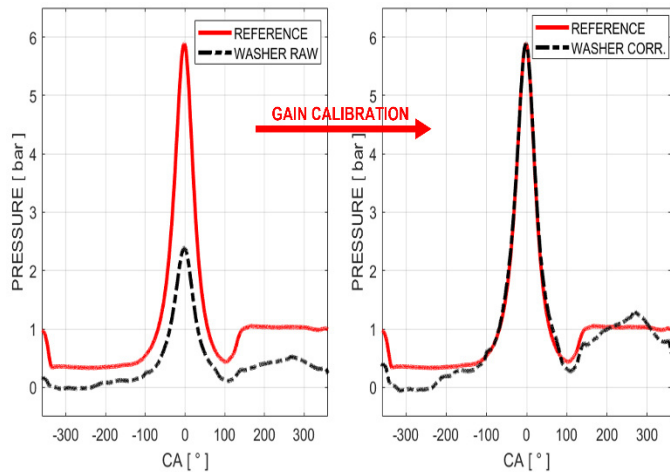

Figure 4. Average pressure curves under motored conditions sensed with the reference sensor and the piezoelectric washer with a pre-calibrated (left-hand graph) and an optimized sensitivity (right-hand graph).

Considering the results achieved with the piezoelectric washer in previous works [19, 29], the combustion indexes are calculated from the washer signal with the same algorithms applied to the reference sensors. Thus, it is possible to define MAWO through the Equation 2:

$$MAWO = \max(|w_{filt}|) \qquad (2)$$

Where w_{filt} is the band-pass filtered washer signal with the same cut-off frequencies adopted for MAPO. In the following paragraphs, the characteristics of the combustion metrics estimated with the piezoelectric washers and the algorithms developed to treat such indexes are described in detail.

Spectrum Analysis

The spectrum of the washer signal is analyzed to verify if the frequency range used to calculate MAPO can be considered valid also for the estimation of MAWO. This study is carried out for the test at 7500 RPM Full-Load, and for the most anticipated SA. This engine point is chosen because both the mechanical noise and the spectrum peaks are high due to knock contribution. In Figure 5 the signal spectrum magnitude of the standard sensors for the considered three cylinders (on which the piezoelectric washer is installed) is shown. The magnitude is the mean one, calculated by averaging the spectrum of 200 cycles.
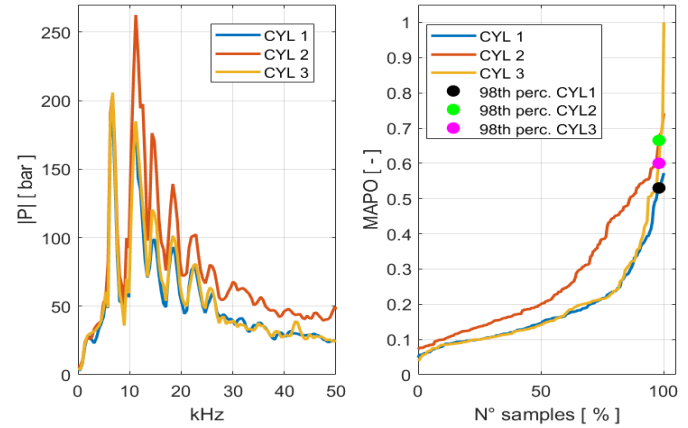

Figure 5. Mean spectrum magnitude of the reference pressure signals (left) and normalized MAPO percentile curves (right).

As expected, combustion chamber harmonics are clearly recognizable for all the in-cylinder pressure sensors. Moreover, it can be noted that the higher the magnitude, the higher the knock intensity, as shown in the percentile curves in the graph on the right. The same analysis is now shown for the piezoelectric washers in Figure 6.
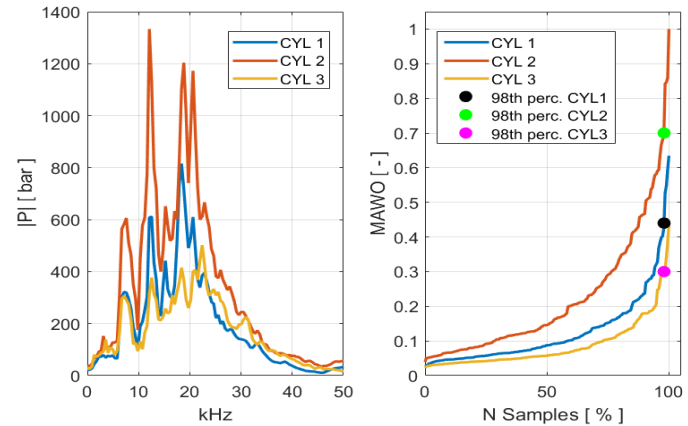

Figure 6. Mean spectrum magnitude of the piezoelectric washer signals (left-hand graph) and the normalized MAWO percentile curves (right-hand graph).

Since the piezoelectric washer sensitivity is calibrated to achieve an in-cylinder pressure curve comparable with that evaluated through the reference sensor, it is expected that even the spectrums are similar. Nevertheless, the harmonics related to the washer signal have an amplitude 2 or 3 times higher than the reference. Such experimental observation can be described with the following considerations or with their combination:

- Since the piezoelectric washer is installed on the engine head it works like an accelerometer, amplifying the vibrations generated by knocking combustions
- The sensitivity can change while the engine is running due to the thermal expansion of the head. This determines a

variation of the spark plug preload, and, consequently, of the washer strain [19, 28].

While the frequency response of the reference sensor has a decreasing trend starting from the first or the second harmonic at most, the mechanical system composed of cylinder head, spark plugs, and piezoelectric washers amplifies the harmonics in the range 10-25 kHz. At the same time, the response of both sensors is included in the frequency range of 5-30 kHz. Such considerations allow to calculate MAWO with the same approach used for MAPO. Moreover, the MAWO values are more spread between all the three considered cylinders, with respect to the MAPO ones, and this is highlighted by the related percentile curves. While the 98th percentile of MAPO (MAPO98) remains in a range of 10% for all three cylinders, the same percentile of MAWO (MAWO98) is in a range of 40-50 %. In other words, due to the different content of the signal of a particular washer in the frequency domain, the correlation between MAPO and MAWO changes for each sensor. Because of all the experimental observations proposed so far, MAWO cannot be directly used to replace MAPO. Such considerations are graphically described in Figure 7, where knock indexes calculated for spark sweeps performed at 7500 RPM full load are shown. Even the knock indexes are normalized for confidentiality reasons, and in the following figures MAPO is divided by the maximum value of the whole database considered in this figure, while MAWO is normalized with respect to the same maximum MAPO.
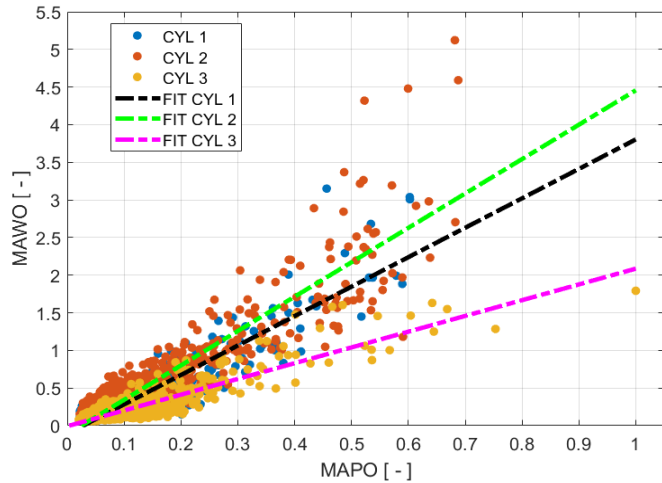

Figure 7. Correlation between normalized MAPO and normalized MAWO for the spark sweep carried out at 7500 RPM at full load.

A model-based, RT algorithm is thus developed to adjust the instantaneous MAWO.

Analysis of the MAWO statistical parameters

As well known, knock is a stochastic phenomenon [30, 31], and it should be analyzed statistically. For fixed engine operating conditions (speed, load, SA and lambda) the statistical distribution of MAPO can be well described with a Gamma or Log-Normal Probability Density Function (PDF) [30]. As described in [20, 22, 27], the Log-Normal PDF fits with high accuracy the probability distribution of such knock intensity index. Moreover, the Log-Normal PDF inherits the characteristics and the properties of the Gaussian PDF and, thus, it needs only two parameters to be completely defined. These parameters are the mean value (μ) and the standard deviation (σ), that can be defined as functions of the 50th and the 98th percentiles of MAPO (MAPO50 and MAPO98, respectively) through the following equations (see the Appendix of [20] for further details):

$$\mu = \log(MAPO\ 50) \tag{3}$$

$$\sigma = \frac{\log(MAPO\ 98) - \mu}{2.0057} \tag{4}$$

Also, MAWO distribution can be described with a Log-Normal PDF. Figure 8 shows MAPO and MAWO histograms, measured for cylinder 1, at the earliest SA at 1500 and 7500 RPM full load. The figure is zoomed to highlight the highest probability values and the lowest MAPO/MAWO.
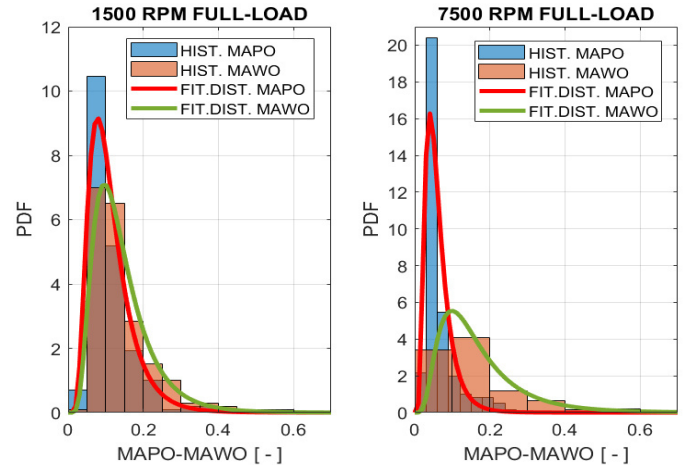

Figure 8. Histograms and the related Log-Normal PDF of the normalized MAPO and MAWO, for the earliest SA value within the spark sweeps carried out at 1500 (left) and 7500 RPM (on the right) full load.

It is important to underline that, increasing the engine speed, the shape of MAWO distribution changes significantly, if compared to MAPO PDF. This means that moving from 1500 to 7500 RPM the coefficients of the correlation function between the instantaneous MAPO and MAWO change. Since it was demonstrated that MAWO PDF can be fitted by a Log-Normal distribution, a comparison between μ and σ of MAPO and MAWO PDSs can be carried out. In Figure 9 the analysis of the correlation of σ is presented for all the three cylinders on which the piezoelectric washer is mounted.
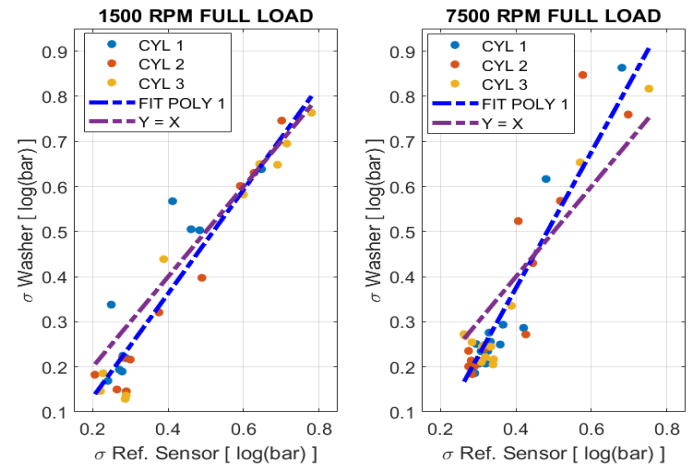

Figure 9. Correlation between the standard deviation of MAPO and MAWO for the spark sweep at 1500 (left) and 7500 RPM (right) full load.

These results demonstrate that σ for the two different knock indexes is comparable. Moreover, the experimental values for all the cylinders are fitted by a first order function that is close to the bisector. This means that such relationship can be defined by Equation 5:

$$\sigma_{MAPO} \approx \sigma_{MAWO} \tag{5}$$

The same analysis is carried out for the mean value and the results are reported in Figure 10.

Figure 10. Correlation between the mean value of MAPO and MAWO for the spark sweeps carried out at 1500 (on the left) and 7500 RPM (on the right) full load.

Considering the results shown in the figures above, the parameter μ of MAWO should be analytically corrected to make it numerically comparable with the MAPO PDF mean value. In other words, the instantaneous MAWO varies as MAPO, accordingly, but each sensor has a particular content in the high-frequency domain of its signal, and this affects the mean value. The aim is to adjust MAWO mean value to make the following equation valid:

$$\mu_{MAPO} = \mu_{MAWO\ CORR.} \tag{6}$$

Where $\mu_{MAWO\ CORR.}$ is the corrected mean value of the MAWO PDF. Considering Equations 3 and 6, it is possible to define the corrective factor K_{corr} as follows:

$$\mu_{MAWO\ CORR.} = \log\left(\frac{MAWO50}{K_{corr}}\right) \tag{7}$$

$$K_{corr} = \frac{MAWO50}{e^{\mu_{MAWO\ CORR.}}} \tag{8}$$

Where MAWO50 is the 50th percentile of MAWO index. Thus, by applying Equation 6, the resulting formulation for K_{corr} is defined by Equation 9 as:

$$K_{corr} = \frac{MAWO50}{e^{\mu_{MAPO}}} \tag{9}$$

Finally, by considering Equation 7, the coefficient calculated via Equation 9 is used to scale the instantaneous MAWO:

$$MAWO_{corr} = \frac{MAWO}{K_{corr}} \tag{10}$$

It is necessary to estimate μ_{MAPO} to properly adjust the instantaneous MAWO value. Since there are several variables that influence the MAPO mean value, the proposed approach to model such parameter is the application of an FNN [27]. While in the previous activity the inputs for the MAPO PDF model were PMAX, engine speed, load, intake air temperature, and the target lambda value, in this work fuel RON is also included. Moreover, the estimation of the MAPO mean value with an intake air temperature different from the nominal value is further developed and improved in this work to make it more robust and accurate under fast transient maneuvers.

MAPO PDF Mean Value Modeling: intake air temperature effects

For fixed engine load, speed, and lambda, it can be stated that the higher the intake air temperature, the higher μ_{MAPO}. In a previous work of the authors [27] an FNN-based model is developed and validated to simulate such quantity and it takes PMAX, engine load, speed, lambda, and intake air temperature as inputs. Figure 11 shows the simulated values of μ_{MAPO} for the spark sweep carried out at 7500 RPM full load and with different intake air temperatures and it can be stated the intake air temperature affects the output values significantly. Nevertheless, the model estimates a higher MAPO mean value for a lower intake air temperature when the expected trend should be the opposite. In other words, the previously developed model is not able to properly capture the effects the air temperature has on the knock intensity.
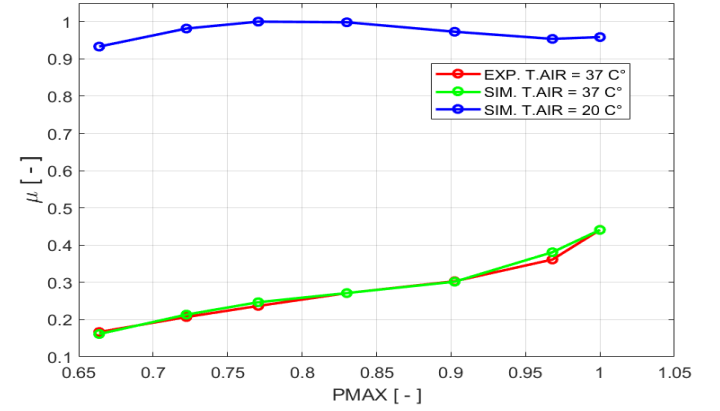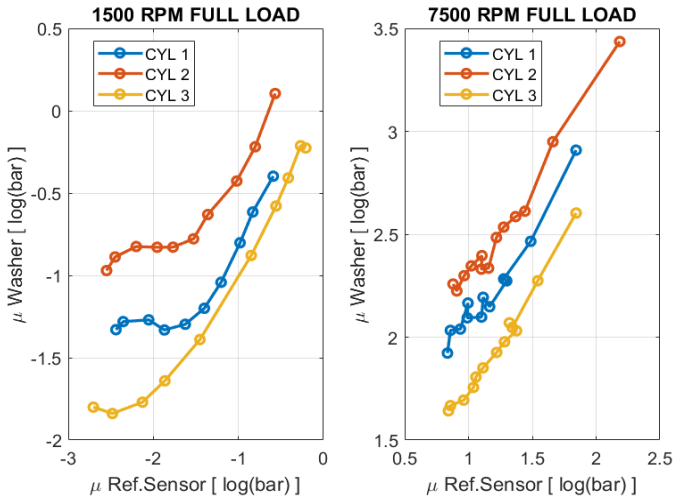

Figure 11. Experimental and simulated values of μ_{MAPO} for the spark sweep carried out at 7500 RPM and full load.

The issue shown in Figure 11 derives from the overfitting of the training dataset [32], for the previous FNN-based model. This phenomenon reduces the accuracy of the model especially when it operates with inputs that are different from those used for the calibration. The main causes of such issue can be divided into two main points [33]:

- Not representative training dataset, or not wide enough
- Issues related to the choice of the neural network inputs

In this case, the spark sweep tests with an intake air temperature higher than the reference have been performed on a limited number of engine points (as shown above in Figure 2) and this is the reason for the poor accuracy of the neural network with respect to such input variable.

The solution proposed to face such issue leads to exclude the intake air temperature from the inputs of the FNN. In this way, the network is trained using as inputs the experimental values of PMAX, engine load, engine speed, and lambda related to the engine points reported in Figure 1. The sensitivity to the intake air temperature is introduced in the μ_{MAPO} model through the definition of an analytical corrective function. Indeed, the FNN network is calibrated for the reference air temperature, and this means that when the experimental temperature is higher than such reference the calculated output is lower than the experimental μ_{MAPO} values. However, it is possible to correlate the simulated and experimental values through a first-degree polynomial as shown in Figure 12.
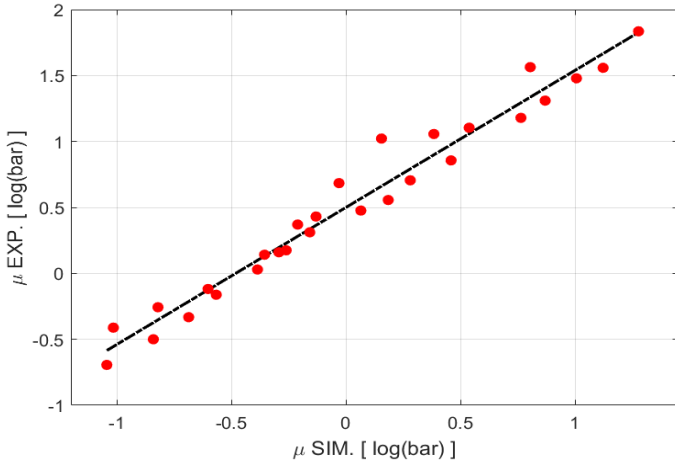
Figure 12. Correlation between simulated and experimental μ_{MAPO} values for the spark sweeps carried out with an intake air temperature of 50 C°, for the four engine points highlighted in red in Figure 2.

Figure 12 highlights that the values are well correlated, and this means that μ_{MAPO} for an intake air temperature of 50 C° can be estimated through the function represented by the black dashed line in Figure 11. The analytical formulation of such function is the following:

$$F_{\mu T.air} = 1.0398 * \mu_{SIM} + 0.5 \qquad (11)$$

Where μ_{SIM} is the output of FNN calibrated for the reference intake air temperature. It is then supposed that the mean value of MAPO PDF varies linearly with respect to the air temperature, following the trend defined by Equation 11, that contains the data for different engine operating conditions. In Figure 13 the block scheme of the μ_{MAPO} model is shown, and the main steps of the calculation are the following ones:

- FNN-based model estimates μ_{MAPO} value for the reference air temperature (μ_{MAPO} T. air Ref.)
- With Equation 11 μ_{MAPO} is determined for the air temperature of 50 C° (μ_{MAPO} 50 C°)
- μ_{MAPO} can be calculated with a first-degree polynomial for the measured intake air temperature (T. air Meas.)
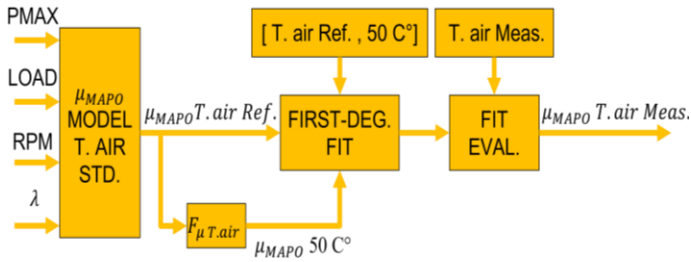

Figure 13. Block scheme of the μ_{MAPO} model with the sensitivity to intake air temperature.

In Figure 14 results of the proposed algorithm are shown for the same experimental data reported in Figure 11.
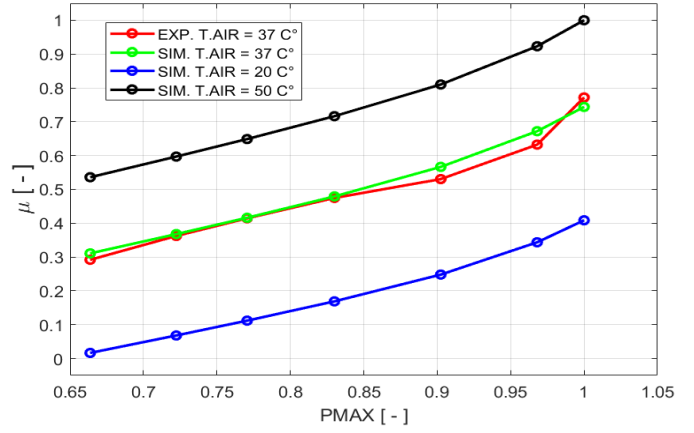

Figure 14 Results of the μ_{MAPO} model for the spark sweep test carried out at 7500 RPM full load, at different intake air temperature values

It can be stated that the model can capture the physical effects of the air temperature on the mean value of the knock intensity. The same approach can be used to introduce the sensitivity to the intake air temperature in the σ_{MAPO} model. The $F_{\mu T.air}$ function is replaced by a $F_{\sigma T.air}$ one.

MAPO PDF Mean Value Modeling: fuel RON effects

This section deals with the introduction of the effect of the fuel quality (i.e. RON) in the μ_{MAPO} model.
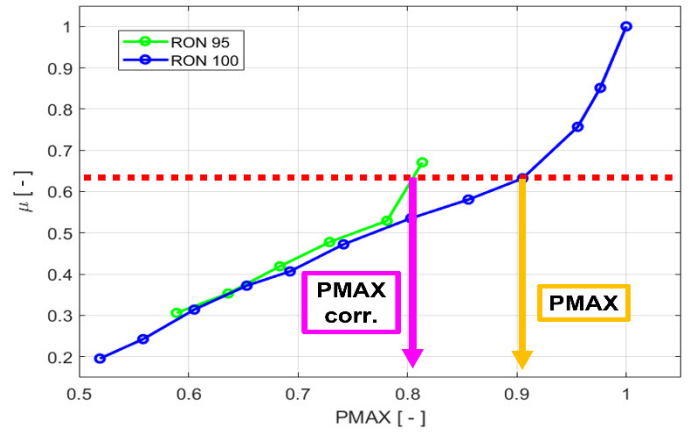

Figure 15. Experimental values of μ_{MAPO} for the spark sweep carried out at 6000 RPM and full load with RON 95 and with RON 100 fuels.

When fuel RON increases, μ_{MAPO} curve maintains the same trend and merely translates towards higher PMAX values. This experimental observation allows to include the effect of a fuel RON variation by changing the value of PMAX used as input for the μ_{MAPO} model described in the previous paragraph. PMAX is modified with the corrective factor K_μ, that is calculated with the following procedure:

- μ_{MAPO} is calculated by using the experimental data of the spark sweep performed with RON 100 gasoline as inputs, and the estimated outputs are thus higher than the experimental ones, because higher PMAX values can be reached without high knock intensity
- K_μ is the PMAX multiplying factor and it is calculated with an automatic optimization procedure that minimizes the following objective function:

$$fo = \sum_{i=1}^{n} |val_{exp.}(i) - val_{sim.}(i)| \qquad (11)$$

Where $val_{exp.}$ and $val_{sim.}$ are experimental and simulated MAPO PDF mean values, respectively.

This procedure leads to calibrate a map of K_μ with respect to the engine speed and load. Figure 16 shows how such map is implemented in the μ_{MAPO} model to estimate the MAPO PDF mean value for the RON 100 gasoline.
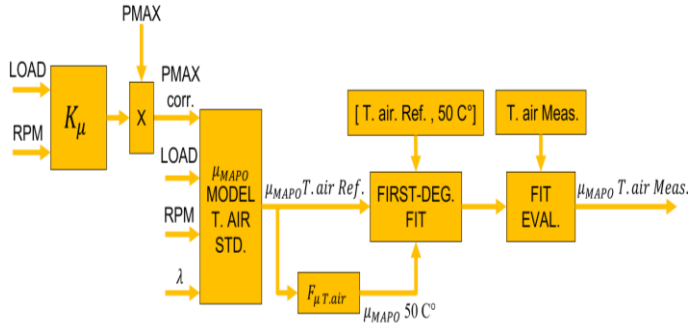

Figure 16. Block scheme of the μ_{MAPO} model for the RON 100 gasoline.

The complete model incudes both the algorithms calibrated for the RON 95 and RON100 gasoline. The resulting μ_{MAPO} for an intermediate fuel RON value is calculated with a linear fitting of μ_{MAPO} values estimated for the RON 95 and 100 gasoline, respectively. Figure 17 presents the correlation between the experimental and the simulated μ_{MAPO} values for all the spark sweeps reported in Figure 1 and Figure 2. R-Square (R2) and Root Mean Square Error (RMSE) are indicated above the figure.
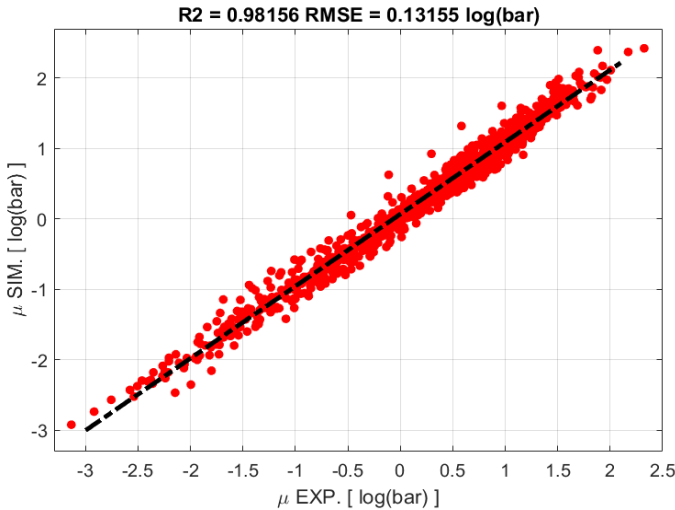

Figure 17. Correlation between the experimental and the simulated μ_{MAPO} for all spark sweeps.

As for the intake air temperature, it is possible to apply the same method to include the sensitivity to fuel RON in the σ_{MAPO} model. In particular, K_μ map is replaced with K_σ, that is calibrated with the same procedure described above.

Maximum In-Cylinder Pressure Modelling

Inputs for the μ_{MAPO} model are some engine variables and a synthetic combustion index (i.e., PMAX). The value of maximum in-cylinder pressure can be evaluated directly from the low-pass filtered washer signal. However, as anticipated above, the approach of the direct PMAX calculation is not reliable, because of the variation of the

sensor sensitivity with respect to the head thermal state and the position on the engine head (see Figure 18). In the following figure the PMAX values are normalized with respect to the maximum of the whole experimental database.
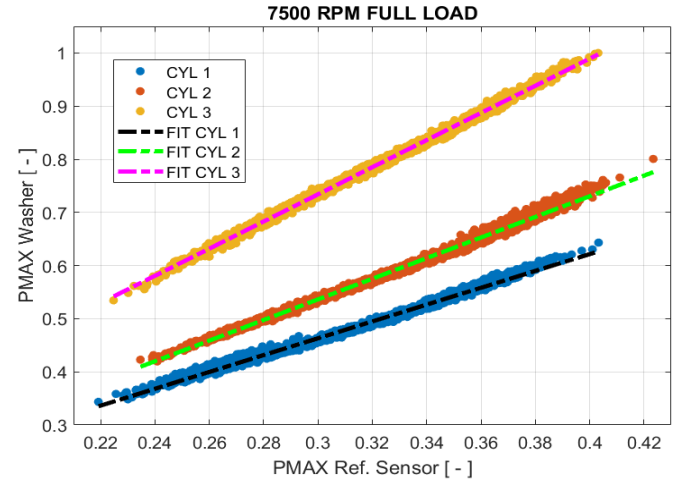

Figure 18. Correlation between the normalized PMAX estimated with the washer and the reference sensor, for the spark sweep carried out at 7500 RPM full load.

For this reason, a model-based approach is implemented to evaluate PMAX and to superpose all the points of Figure 18 on the bisector. This model is based on the algorithm developed and validated in [21]. Such function uses the engine load (defined as the trapped air mass per cycle, per cylinder) and the MFB50. Nevertheless, several washer combustion indexes can be directly correlated to the combustion phase measured with the reference sensor:

- MFB50
- MFB10
- Angle of PMAX (APMAX)

It is thus evaluated which is the most robust for the PMAX estimation on the entire engine operating range. The block scheme of the resulting algorithm, with the PMAX estimation as well, is shown in Figure 19. Two buffers are implemented in the algorithm: one is needed to calculate MAWO50, while the other is used to calculate a filtered value of PMAX to reduce the effect of the CCV. The size of these buffers needs to be calibrated to maximize the correlation between MAPO and the corrected MAWO values.

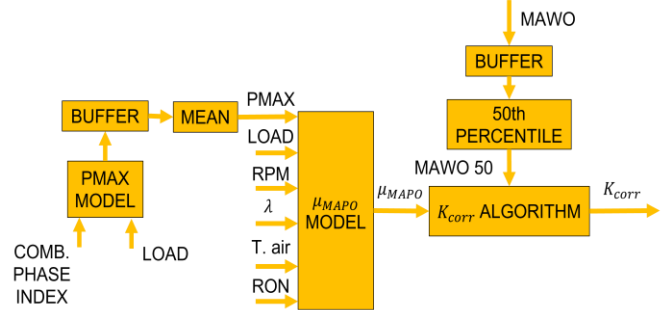Figure 19. The block scheme of the complete algorithm for the K_{corr} calculation.

The three combustion phase indexes mentioned above are calculated from the washer signal and they are considered to directly estimate the combustion phase (i.e., the MFB50). The values achieved by analyzing all the spark sweep tests referred to Figure 3 are concatenated for all the cylinders and are reported in Figure 20.
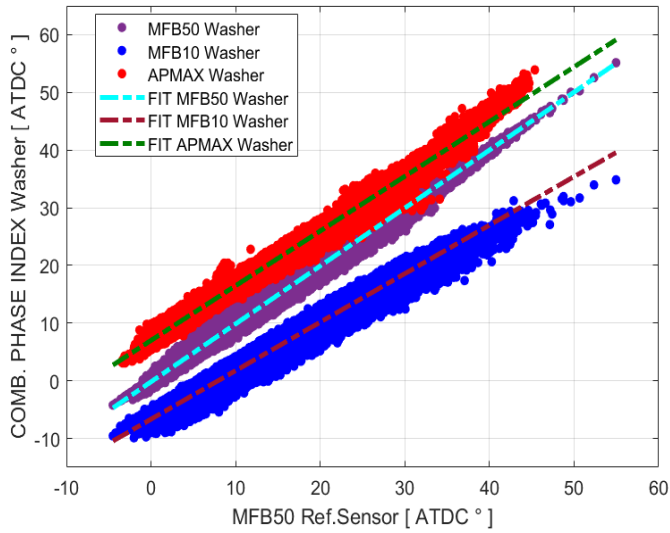
Figure 20. Correlation between the piezoelectric washer combustion phase indexes obtained for all the spark sweep tests and the MFB50 calculated from the reference signal.

The results show how all the three indexes are reliable for the estimation of the MFB50 on the entire engine operating field. In Table 3, the RMSE and the R2 are reported for each correlation.

Table 3. RMSE and R2 of the correlation between the washer combustion phase indexes and the reference MFB50.

Model Layout	R2	RMSE
MFB50 Washer – MFB50 Ref. Sensor	0.9818	1.12 °
MFB10 Washer – MFB50 Ref. Sensor	0.9640	1.59 °
APMAX Washer – MFB50 Ref. Sensor	0.9826	1.11 °

Model performance is evaluated by comparing accuracy of calculated PMAX values using the three different combustion phase indexes as input. Of course, since PMAX model is calibrated for taking the reference MFB50 as input, a linear polynomial is required to convert the MFB10 or APMAX into the MFB50. Such functions for MFB10 and APMAX are obtained by reversing those shown in Figure 20. In Figure 21, PMAX values calculated by taking the MFB50 of the washer as input are shown for the spark sweep at 7500 RPM full load, for the three considered cylinders.
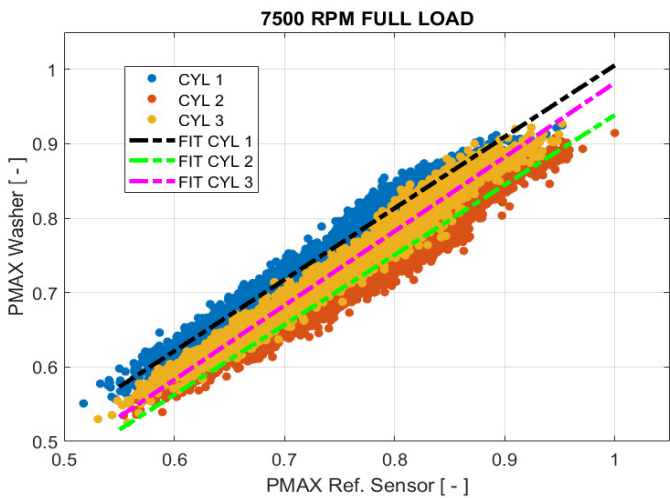

Figure 21. Estimated normalized PMAX using MFB50 from the washer signal for the spark sweep performed at 7500 RPM full load, for the three cylinders.

The calculated PMAX is accurate especially for the cylinder 1 and the fitting polynomial is close to the bisector. It is not the same for

cylinders number 2 and 3 and, for the latter, the PMAX is underestimated by 10 %. Such difference has relevant consequences on the MAPO PDF mean value model accuracy. Indeed, $\mu_{MAWO\ CORR.}$ values are not aligned along the bisector of the μ_{MAPO} - $\mu_{MAWO\ CORR.}$ graph, as shown in Figure 22.
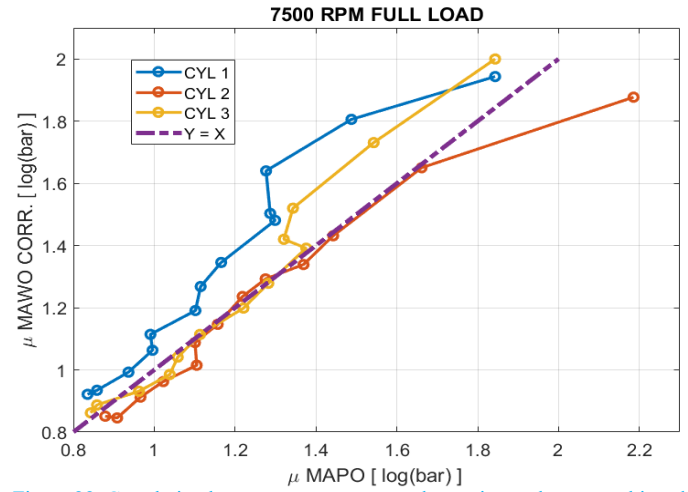

Figure 22. Correlation between $\mu_{MAWO\ CORR.}$ and experimental μ_{MAPO} achieved by feeding the MAPO mean value model with the PMAX estimated directly from the washer MFB50, for the spark sweep performed at 7500 RPM full load.

The same analysis is carried out by using alternatively the MFB10 and the APMAX estimated from the washer pressure signal. In Figure 23 the results for the spark sweep at 7500 RPM full load are reported and it can be stated that the maximum-in-cylinder pressure is underestimated by around 5%, especially at the highest PMAX values. At the same time, the differences between correlation functions of the three cylinders are lower than the observed in Figure 21. $\mu_{MAWO\ CORR.}$ values are thus well correlated with the μ_{MAPO} ones and superposed along the bisector. This means that Equation 6 is verified with this approach, let alone the very highest values of PMAX, especially with the MFB10 as input.
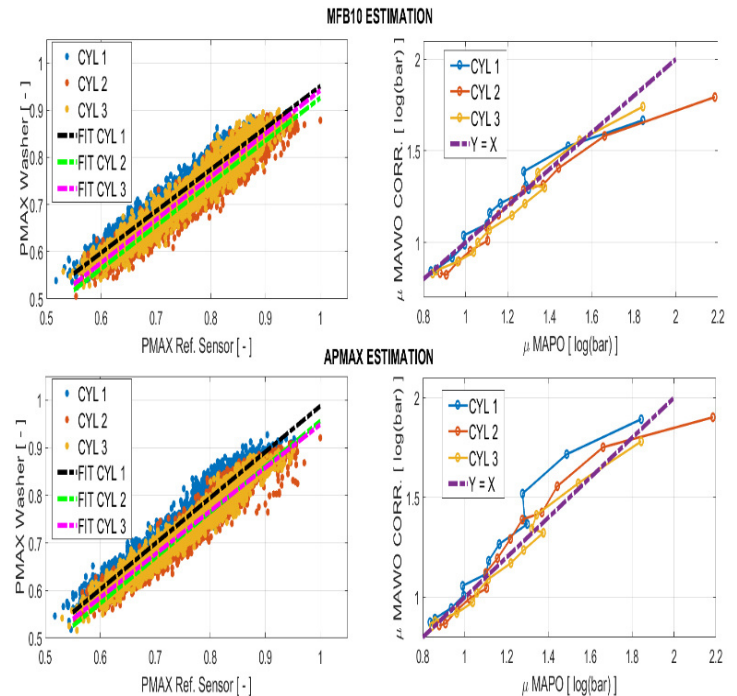

Figure 23. Correlation between the estimated and the experimental normalized PMAX (graphs on the left) and correlation between $\mu_{MAWO\ CORR.}$ and μ_{MAPO}

(right-hand side graphs) for the spark sweep carried out at 7500 RPM and full load.

Table 4 reports RMSE between the calculated and the experimental PMAX. The values reported in such table are the average between the three cylinders for all the spark sweeps and, thus, they represent the mean error for the PMAX calculation on the entire engine operating field. Since the results achieved with the MFB50 showed the issues described above, the MFB10 is selected as the index for the combustion phase determination. Although, the accuracy improvement is not significative (RMSE is close to the other values) and, in this way, the calculation of $\mu_{MAWO\ CORR.}$ is more robust (as shown by the correlation in Figure 23).

Table 4. RMSE between the calculated and the experimental PMAX when the model is fed with different combustion phase indexes estimated from the washer signal.

Model Layout	RMSE
PMAX MFB50 Washer	2.27 bar
PMAX MFB10 Washer	3.33 bar
PMAX APMAX Washer	3.08 bar

Validation under steady-state conditions

The resulting algorithm for the RT correction of the combustion and knock indexes estimated from the washer signal is implemented in a RCP system, for the verification at the engine test bench. Such system receives the main engine operating parameters, instantaneous combustion indexes (both from reference sensors and washers) via a Controller Area Network (CAN) communication protocol, from the ECU and the indicating system, respectively. In this way the algorithm can be tested online, and the adjusted instantaneous washer indexes can be recorded perfectly synchronized with those of the reference sensors. For the validation under steady-state conditions, the two buffers shown in Figure 19 are composed of 200 elements. A new spark sweep is performed on the engine test bench at 7500 RPM full load. The results are shown in Figure 24, where the reported fitting function is not related to a single cylinder, but it considers all the values reported in the figure.
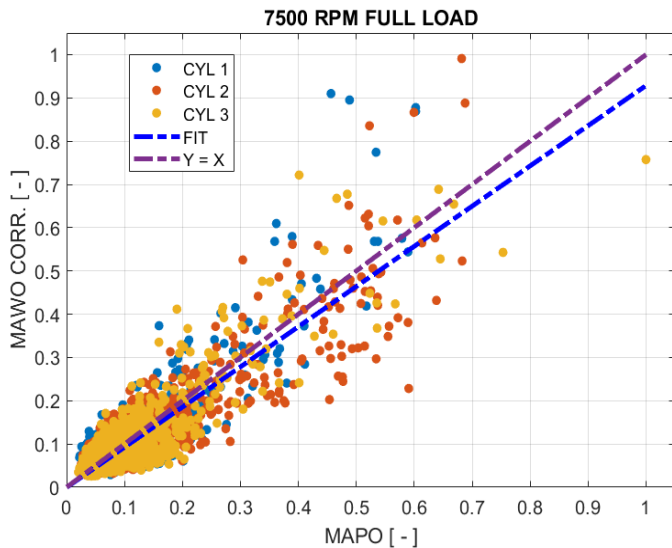

Figure 24. Correlation between the normalized adjusted MAWO and the normalized experimental MAPO.

While the correlation shown in Figure 7 is different for each cylinder, the adjusted MAWO values have now the same trend and, moreover, the fitting function is closed to the bisector. Figure 25 reports the results achieved by applying the described algorithm to all the data

acquired during the experimental champaign referred to Figure 3. In this figure, for each engine operating condition, MAPO and MAWO for the three cylinders equipped with the piezoelectric washers are indicated with the same color.
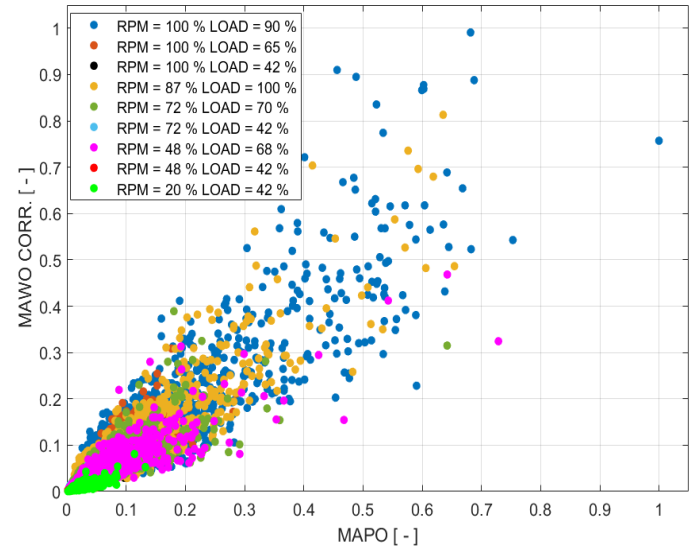

Figure 25. Correlation between the experimental MAPO and the adjusted MAWO for other tested engine points.

The R2 between all the experimental MAPO values and the corrected MAWO shown in Figure 25 is equal to 0.82, and it is representative for the whole engine operating filed. This value can be considered as a confirmation of the high model accuracy. As well-known, due to knock stochastic nature, the high-frequency high pressure oscillations measurement is strongly affected by the sensor position. Even using the same kind of sensor mounted in different positions of the combustion chamber, it is common calculating R2 values for the correlation between the instantaneous MAPO close to 0.7-0.8 (see the Appendix for an analysis of the results achieved with the reference sensor and the measuring spark plug). Of course, even in this case, the reference sensor and the piezoelectric washer are mounted in different positions of the engine head, and this is the reason why an R2 equal to 0.82 is considered a demonstration of the robustness and the accuracy of the proposed methodology. Considering the results reported in [18] in which the same range of the engine speed investigated in this work is considered, R2 values equal to 0.86 for the accelerometers and 0.79 for microphones are reported. The main benefits brought by the application of the washers are related to the installation (that does not imply relevant design changes of the engine head) and using the signal of each cylinder for the estimation (and the control) of all the main combustion metrics (and not only the knock intensity). More generally, the cost of the sensor, the impact, and the reliability of the installation on the vehicle have to be considered when the proposed solution is compared to the other technologies mentioned above.

Validation under transient conditions

The results presented in this section are achieved by reproducing a transient maneuver at the engine test bench, with which the speed and the load increase in a very fast way. The algorithm for the RT correction of the washer indexes is executed on a RCP system. In Figure 26 the profiles of the pedal and the engine speed are shown. Also in this case, the combustion and knock indexes estimated from the reference sensors and the adjusted values of the piezoelectric washers are recorded with the RCP machine. In this way, the instantaneous values are directly comparable to validate the developed functions.
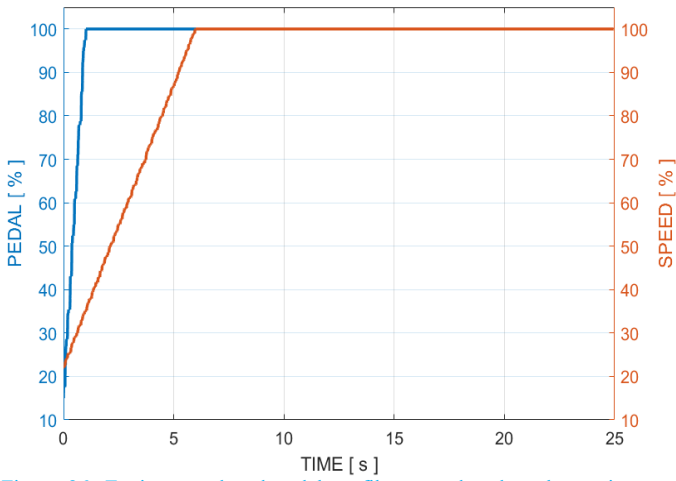
Figure 26. Engine speed and pedal profiles reproduced at the engine test bench to validate the developed algorithm under transient conditions.

As mentioned before, under transient conditions the length of the PMAX and MAWO buffers affect the algorithm accuracy. Such parameter is calibrated, and the optimization process is carried out with a Design of Experiment (DoE) approach, varying the length of the buffers. The value that maximizes the R2 between the MAPO and the adjusted MAWO is applied.

In Figure 27 the correlation between MAPO and adjusted MAWO recorded during the test is reported. As for Figure 24, the fitting function reported in the following figure refers to the total amount of engine points and not to a specific cylinder.
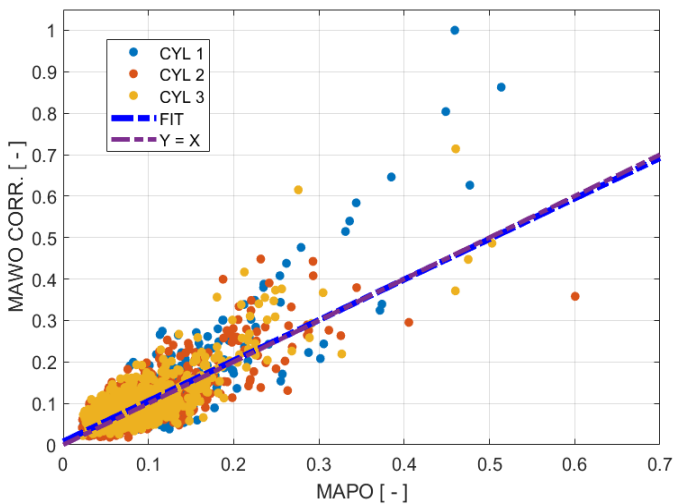

Figure 27. Correlation between the experimental MAPO and the corrected MAWO for the test under transient conditions.

The results are very similar to those achieved under steady-state conditions. It can be noted that the algorithm is very accurate for the lowest normalized MAPO values, while the accuracy is lower for the highest levels of knock. This is because the combustion cycles characterized by high MAPO values excite the natural frequencies of the mechanical system composed by the engine head, the spark plug and the piezoelectric washer, generating high oscillations in the high frequency range of the signal spectrum, that are superposed to the content produced by knock. However, to further verify the accuracy of the functions, the curves of the sorted MAPO and MAWO are compared for each cylinder, as shown in Figure 28. The values are normalized with respect to the maximum MAPO or MAWO recorded for each cylinder.
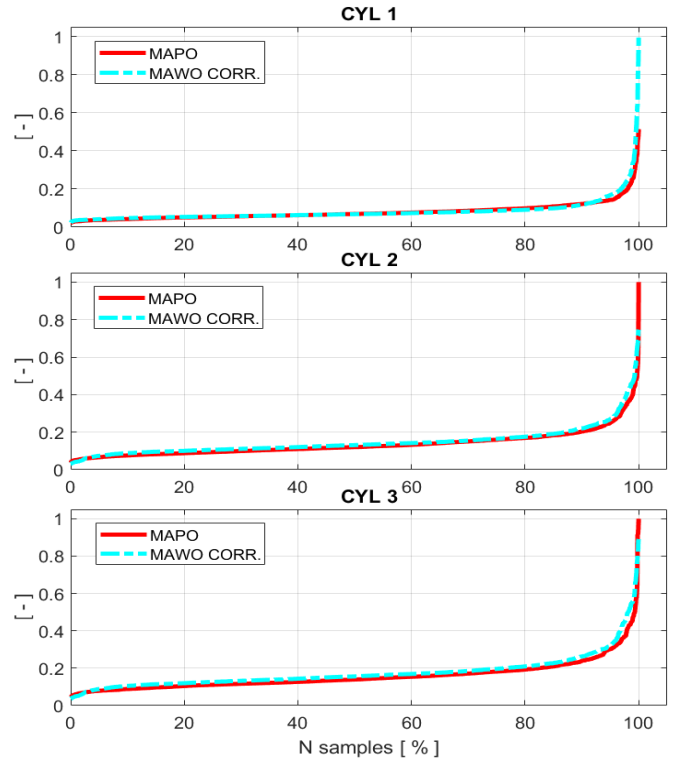

Figure 28. The curves of the sorted MAPO and the adjusted MAWO for the tests under transient conditions.

The following table reports the percentage error between the main percentile values of the MAPO and the adjusted MAWO recorded during such test. The negative values mean that the corrected MAWO is lower than MAPO, and vice versa.

Table 5. The error between the percentile values of the MAPO and the adjusted MAWO.

Percentile value	CYL 1	CYL 2	CYL 3
50	- 1 %	1 %	1 %
95	2 %	2 %	2 %
98	5 %	5 %	8 %
99	9 %	6 %	9 %
100	50 %	-26 %	-11 %

Only for the 100th percentile the absolute value of the error is higher than 10%. Thus, the results demonstrate the developed algorithm is robust and accurate and the piezoelectric washers can be applied to estimate all the main combustion and knock indexes, independently from the sensitivity of the particular sensor and the position on the engine head.

Conclusions

In the first part of this work a comparison between the spectrum of the high-pass filtered signals of the in-cylinder pressure sensors, taken as reference, and the piezoelectric washer is performed. Both sensors show the content due to knocking combustion in the same range of frequencies and this allows to treat both signals in the same way, for the calculation of the knock intensity index.

The statistical properties of the MAWO are analyzed and it is demonstrated the Log-Normal PDF can be used to accurately describe its trend, for fixed engine operating conditions. The mean value and the standard deviation of MAPO and MAWO PDFs are compared for fixed engine operating conditions (engine speed, load and SA). While the standard deviation is comparable for both such indexes, the mean value of MAWO needs to be properly adjusted, due to the particular high-frequency content of the signal spectrum. The main aim of this paper is the development and the validation of

the algorithm to calculate such scaling factor K_{corr} that is based on the MAPO mean value modeling. A Feedforward Neural Network-based approach has been implemented for the MAPO mean value modeling and the algorithm for the calculation of the MAWO scaling factor is developed.

The reliability of the main combustion phase indexes estimated from the washer signal is investigated and the MFB10 is finally chosen to feed the PMAX model, needed by the MAPO mean value model as input.

In the last part of the work, the proposed algorithm for the correction of the instantaneous MAWO is validated for both the steady-state and transient conditions. It has been demonstrated that a correlation coefficient (R2) equal to 0.82 between the experimental MAPO and the adjusted MAWO can be achieved with the described method.

The algorithm is then validated under transient conditions reproducing a real vehicle maneuver at the engine test bench. The algorithm for the RT correction of the washer indexes is executed on an RCP system and the indexes of the reference sensor are directly compared with the adjusted indexes of the washer. The results show that the piezoelectric washer can be applied to accurately estimate the main combustion metrics. Hence, the reliability of this sensor and the low cost (for both the production and the installation on the engine head) make the proposed system a viable solution to develop a technology suitable for the on-vehicle applications.

The system composed by the washers and the model-based function for the estimation of MAPO, PMAX and MFB50 will be further validated by implementing the algorithm in a development ECU and testing it on a prototyping vehicle.

References

1. Scala, F., Galloni, E., and Fontana, G., "Numerical Analysis of a Spark-Ignition Engine Fueled by Ethanol-Gasoline and Butanol-Gasoline blends: Setting the Optimum Spark Advance," SAE Technical Paper 2017-24-0117, 2017, doi:10.4271/2017-24-0117.
2. Taglialatela, F., Cesario, N., Porto, M., Merola, S. et al., "Use of Accelerometers for Spark Advance Control of SI Engines," *SAE Int. J. Engines* 2(1):971-981, 2009, doi: 10.4271/2009-01-1019.
3. Cavina, N., Poggio, L., and Sartoni, G., "Misfire and Partial Burn Detection based on Ion Current Measurement," *SAE Int. J.Engines* 4(2):2451-2460,2011, doi:10.4271/2011-24-0142.
4. Cavina, N., Rojo, N., Businaro, A., and Cevolani, R., "Comparison between Pressure- and Ion-Current-Based Closed-Loop Combustion Control Performance," *SAE Int. J.Engines* 12(2):219–230, 2019, doi:10.4271/03-12-02-0016.
5. Liu, Y., Li, L., Lu, H., Deng, J. et al., "In-Cycle Knocking Detection and Feedback Control Based on In-Cylinder Pressure and Ion Current Signal in a GDI Engine," SAE Technical Paper 2016-01-0816, 2016, doi:10.4271/2016-01-0816.
6. Cavina, N., Rojo, N., Poggio, L., Calogero, L. et al., "Investigation on Pre-Ignition Combustion Events and Development of Diagnostic Solutions Based on Ion Current Signals," *SAE Int. J. Engines* 10(4):2017, doi:10.4271/2017-01-0784.
7. Wang, J., Hu, Z., Zhu, D., Ding, W. et al., "In Cycle Pre-Ignition Diagnosis and Super-Knock Suppression by Employing Ion Current in a GDI Boosted Engine," SAE Technical Paper 2020-01-1148, 2020, doi:10.4271/2020-01-1148.
8. Grimaldi, A., Mucciarella, L., and Virgilii, F., "Study of Ion Current Based Misfire Detection in Motorcycle Applications," SAE Technical Paper 2017-32-0011, 2017.
9. Doi, K., Nakamura, Y., Hanashi, K. and Hashizume, K., "Development of Spark Plug for Ion Current Misfire Detection System," *SAE Int. J. Engines* 5(3):2012, doi:10.4271/2012-01-1253.
10. Kusuhara, T., Shinkai, T., Yoshida, K., Langley, D. et al., "Development on Internal EGR Feedback Control Based on Ion Current," SAE Technical Paper 2017-01-0793, 2017, doi:10.4271/2017-01-0793.
11. Andrea Businaro, Nicolò Cavina, Enrico Corti, Giorgio Mancini, Davide Moro, Fabrizio Ponti, Vittorio Ravaglioli, Accelerometer Based Methodology for Combustion Parameters Estimation, Energy Procedia, Volume 81, 2015, Pages 950-959, ISSN 1876-6102, doi.org/10.1016/j.egypro.2015.12.152.
12. Fabrizio Ponti, Vittorio Ravaglioli, Enrico Corti, Davide Moro, Matteo De Cesare, Remote Combustion Sensing Methodology for Non-Intrusive Cylinder Pressure Estimation in Diesel Engines, IFAC Proceedings Volumes, Volume 46, Issue 21, 2013, Pages 353-359, ISSN 1474-6670, ISBN9783902823489, doi.org/10.3182/20130904-4-JP-2042.00039.
13. Amezcua, E.R., Maldonado, B., Rothamer, D., Kim, K. et al., "Accelerometer-Based Estimation of Combustion Features for Engine Feedback Control of Compression-Ignition Direct-Injection Engines," SAE Technical Paper 2020-01-1147, 2020, doi.org/10.4271/2020-01-1147.
14. Ranuzzi, F., Cavina, N., Scocozza, G., Brusa, A. et al., "Experimental Validation of a Model-Based Water Injection Combustion Control System for On-Board Application," SAE Technical Paper 2019-24-0015, 2019, https://doi.org/10.4271/2019-24-0015.
15. Rosas, M. and Amador, G., "Knock Detection Method for Dual-Fuel Compression Ignition Engines Based on Block Vibration Analysis," *SAE Int. J. Engines* 14 (2) : 199 - 209 , 2021 , doi.org/10.4271/03-14-02-0012 .
16. Siano, D., Bozza, F., D'Agostino, D., and Panza, M., "The Use of Vibrational Signals for On-Board Knock Diagnostics Supported by In-Cylinder Pressure Analyses," SAE Technical Paper 2014-32-0063, 2014, doi.org/10.4271/2014- 32-0063.
17. Cavina, N., Businaro, A., De Cesare, M., and Paiano, L., "Knock Control Based on Engine Acoustic Emissions: Calibration and Implementation in an Engine Control Unit," SAE Technical Paper 2017-01-0785, 2017, doi.org/10.4271/2017-01-0785.
18. Cavina, N., Businaro, A., De Cesare, M., Monti, F. et al., "Application of Acoustic and Vibration-Based Knock Detection Techniques to a High Speed Engine," SAE Technical Paper 2017-01-0786, 2017, doi.org/10.4271/2017-01-0786.
19. Corti E., Abbondanza M., Ponti F., Raggini L., "The Use of Piezoelectric Washers for Feedback Combustion Control", SAE Int. Journal of Advances and Current Practices in Mobility, doi.org/10.4271/2020-01-1146
20. Cavina, N., Brusa, A., Rojo, N., and Corti, E., "Statistical Analysis of Knock Intensity Probability Distribution and Development of 0-D Predictive Knock Model for a SI TC Engine," SAE Technical Paper2018-01-0858, 2018, doi.org/10.4271/2018-01-0858.
21. Scocozza, G., Silvagni, G., Brusa, A., Cavina, N. et al., "Development and Validation of a Virtual Sensor for Estimating the Maximum in-Cylinder Pressure of SI and GCI Engines," SAE Technical Paper 2021-24-0026, 2021, https://doi.org/10.4271/2021-24-0026.
22. Brusa, A., Cavina, N., Rojo, N., Cucchi, M. et al., "Development and Validation of a Control-Oriented Analytic Engine Simulator," SAE Technical Paper 2019-24-0002, 2019, https://doi.org/10.4271/2019-24-0002.
23. Brusa, A.; Cavina, N.; Rojo, N.; Mecagni, J.; Corti, E.; Ravaglioli, V.; Cucchi, M.; Silvestri, N. Development and Experimental Validation of an Adaptive, Piston-Damage-Based Combustion Control System for SI Engines: Part 1—Evaluating Open-Loop Chain Performance. Energies 2021, 14, 5367. doi.org/10.3390/en14175367

24. Brusa, A.; Cavina, N.; Rojo, N.; Mecagni, J.; Corti, E.; Moro, D.; Cucchi, M.; Silvestri, N. Development and Experimental Validation of an Adaptive, Piston- Damage- Based Combustion Control System for SI Engines: Part 2–Implementation of Adaptive Strategies. *Energies* 2021, *14*, 5342. doi.org/10.3390/en14175342

25. Matlab Documentation, The MathWorks, 2020, https://www.mathworks.com/.

26. Egan, D., Koli, R., Zhu, Q., and Prucka, R., "Use of Machine Learning for Real-Time Non-Linear Model Predictive Engine Control," SAE Technical Paper 2019-01-1289, 2019, doi.org/10.4271/2019-01-1289.

27. Mecagni, J., Brusa, A., Cavina, N., Ponti, F. et al., "Model-Based Exhaust Gas Temperature Control to Reduce the Mixture Enrichment at High Loads," SAE Int. J. Engines 16(3):2023.

28. Hoth, A., Pulpeiro Gonzalez, J., Kolodziej, C., and Rockstroh, T., "Effects of Lambda on Knocking Characteristics and RON Rating," *SAE Int. J. Adv. & Curr. Prac. in Mobility* 1(3):1188-1201, 2019, doi.org/10.4271/2019-01-0627.

29. Corti, E., Raggini, L., Rossi, A., Brusa, A. et al., "Application of Low-Cost Transducers for Indirect In-Cylinder Pressure Measurements," *SAE Int. J. Engines* 16(2):2023, doi.org/10.4271/03-16-02-0013.

30. Ghandhi, J. and Kim, K., "A Statistical Description of Knock Intensity and Its Prediction," SAE Technical Paper 2017-01-0659, 2017, doi.org/10.4271/2017-01-0659.

31. Peyton J., Spelina, J., and Frey, J., "Control-Oriented Knock Simulation," *SAE Int. J. Engines* 9(2):2016, doi:10.4271/2016-01-0821

32. S. Lawrence and C. L. Giles, "Overfitting and neural networks: conjugate gradient and backpropagation," *Proceedings of the IEEE-INNS-ENNS International Joint Conference on Neural Networks. IJCNN 2000. Neural Computing: New Challenges and Perspectives for the New Millennium*, 2000, pp. 114-119 vol.1, doi: 10.1109/IJCNN.2000.857823.

33. Ying, Xue. (2019). An Overview of Overfitting and its Solutions. Journal of Physics: Conference Series. 1168. 022022. doi:10.1088/1742-6596/1168/2/022022.

Definitions/Abbreviations

ANN	Artificial Neural Network
CCV	Cycle-to-Cycle Variation
DoE	Design of Experiment
ECU	Engine Control Unit
FNN	Feedforward Neural Network
GDI	Gasoline Direct Injection
ION	Ionization Current
MAPO	Maximum Amplitude of Pressure Oscillation
MAWO	Maximum Amplitude of Washer Oscillation
MBT	Maximum Brake Torque
MFB10	10% of Mass Fraction Burned
MFB50	50% of Mass Fraction Burned
MFB90	90% of Mass Fraction
NN	Neural Network
PDF	Probability Density Function
R2	R-Square
RCP	Rapid Control Prototyping
RMSE	Root Mean Square Error
RON	Research Octane Number
RT	Real Time
SA	Spark Advance
SI	Spark Ignition
SOC	Start of Combustion
WOT	Wide Open Throttle

APPENDIX

Knock intensity measurement is strongly affected by the position of the sensor in the combustion chamber. Some experimental tests are performed with the same experimental setup and with the measuring spark plugs mounted on two cylinders (the main characteristics of these sensors are reported in Table 6).

Table 6. Main features of the piezoelectric sensor installed in the measuring spark plug

Sensitivity	10 Pc/bar
Pressure range	0 – 200 bar
Overload	250 bar
Natural frequency	≈ 65 kHz

Such tests consist of spark sweeps and the final aim is that to compare the instantaneous MAPO calculated from the signal of these two kinds of commercial sensor. In this way, it has been verified the R2 value of the correlation between the reference MAPO and that estimated with a piezoelectric sensor installed in the same position of the washers (i.e., in correspondence of the side-mounted spark plugs).

During these spark sweep, 300 engine cycles are recorded for each actuated SA. MAPO is calculated for both the signals with the Equation 1 and with the same cut-off frequencies. In the following figure, the correlation between the MAPO calculated for both the sensors and for the two cylinders is reported. As expected, sensing the knock intensity in different areas of the combustion chamber leads to record different content in the high-frequency domain of the signal and, thus, the R2 value is typically close to 0.7-0.8, even for commercial sensors.
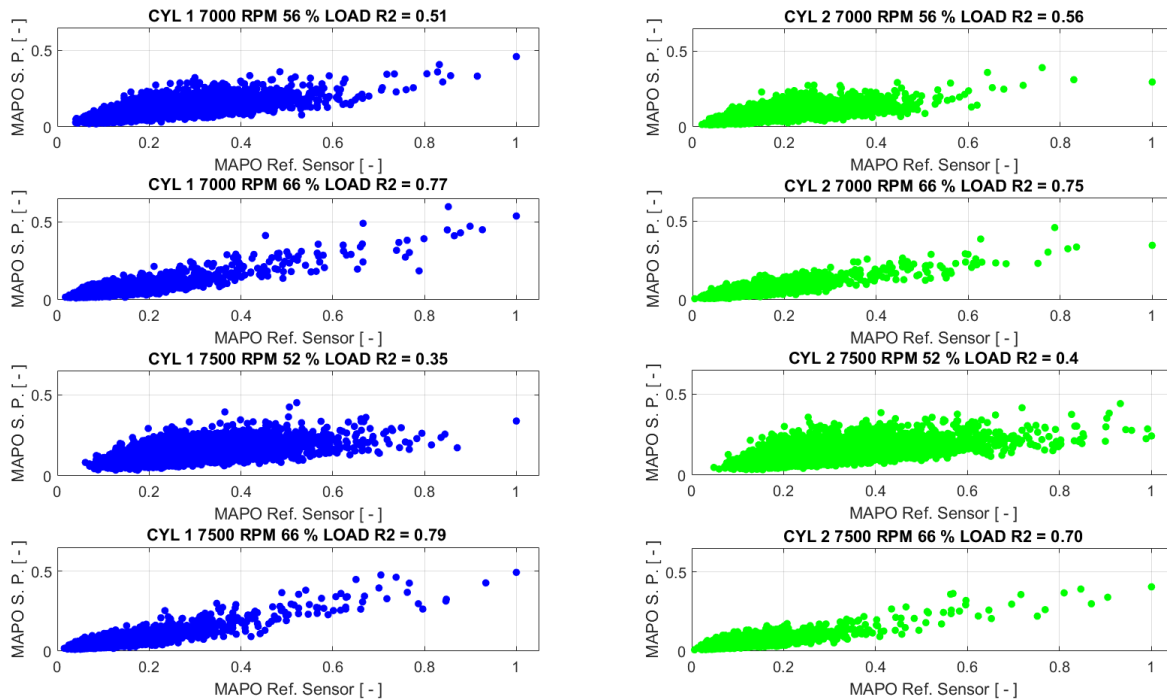

Figure A1. Correlation between the MAPO values calculated from the signal of the reference sensor and the measuring Spark Plug (S.P.).